# Vibrational Spectroscopy of the G···C Base Pair: Experiment, Harmonic and Anharmonic Calculations, and the Nature of the Anharmonic Couplings

**Brina Brauer,[†] R. Benny Gerber,[*,†,‡] Martin Kabeláč,[§] Pavel Hobza,[§] Joost M. Bakker,[||] Ali G. Abo Riziq,[⊥] and Mattanjah S. de Vries[⊥]**

*Department of Physical Chemistry and Fritz Haber Research Center, The Hebrew University of Jerusalem, Jerusalem 91904, Israel, Department of Chemistry, University of California, Irvine, California 92697, Institute of Organic Chemistry and Biochemistry, Academy of Sciences of the Czech Republic and Center for Biomolecules and Complex Molecular Systems, Flemingovo nám. 2, 16610 Prague 6, Czech Republic, FOM Institute for Plasmaphysics Rijnhuizen, Edisonbaan 14, NL-3439 MN Nieuwegein, The Netherlands, and Department of Chemistry and Biochemistry, University of California, Santa Barbara, California 93106-9510*

*Received: April 6, 2005; In Final Form: May 30, 2005*

The results of harmonic and anharmonic frequency calculations on a guanine−cytosine complex with an enolic structure (a tautomeric form with cytosine in the enol form and with a hydrogen at the 7-position on guanine) are presented and compared to gas-phase IR−UV double resonance spectral data. Harmonic frequencies were obtained at the RI-MP2/cc-pVDZ, RI-MP2/TZVPP, and semiempirical PM3 levels of electronic structure theory. Anharmonic frequencies were obtained by the CC-VSCF method with improved PM3 potential surfaces; the improved PM3 potential surfaces are obtained from standard PM3 theory by coordinate scaling such that the improved PM3 harmonic frequencies are the same as those computed at the RI-MP2/cc-pVDZ level. Comparison of the data with experimental results indicates that the average absolute percentage deviation for the methods is 2.6% for harmonic RI-MP2/cc-pVDZ (3.0% with the inclusion of a 0.956 scaling factor that compensates for anharmonicity), 2.5% for harmonic RI-MP2/TZVPP (2.9% with a 0.956 anharmonicity factor included), and 2.3% for adapted PM3 CC-VSCF; the empirical scaling factor for the ab initio harmonic calculations improves the stretching frequencies but decreases the accuracy of the other mode frequencies. The agreement with experiment supports the adequacy of the improved PM3 potentials for describing the anharmonic force field of the G···C base pair in the spectroscopically probed region. These results may be useful for the prediction of the pathways of vibrational energy flow upon excitation of this system. The anharmonic calculations indicate that anharmonicity along single mode coordinates can be significant for simple stretching modes. For several other cases, coupling between different vibrational modes provides the main contribution to anharmonicity. Examples of strongly anharmonically coupled modes are the symmetric stretch and group torsion of the hydrogen-bonded $NH_2$ group on guanine, the OH stretch and torsion of the enol group on cytosine, and the NH stretch and NH out-of-plane bend of the non-hydrogen-bonded NH group on guanine.

## I. Introduction

Recent advances in experimental techniques have permitted the spectroscopic study of biological molecules in the gas phase, thereby leading to a deeper understanding of the forces and dynamics influencing biological processes.[1] For example, ultraviolet and infrared experiments have allowed the determination of amino acid[2] and peptide conformations[3] and the exploration of nucleic acid base tautomerization and pairing.[4] In addition, computational costs are continually decreasing, so that accurate computations of molecular potential surfaces, properties, and dynamics are beginning to be performed for biological molecules. When used together, the availability of gas-phase spectroscopic data can aid in improving theoretical methods of calculation for biological molecules, while accurate computational methods can aid in spectroscopic identification of biological conformers and their properties.

The structure of nucleic acid base pairs and, in particular, the hydrogen bonding between the pairs has been of interest since the base pair structures were first described.[5] A relationship between the presence of tautomeric forms of the bases and spontaneous mutation in DNA was proposed just after the structure of DNA was described.[6] It has since been the subject of both theoretical and experimental study;[7] however, the relationship between the tautomerization of base pairs and DNA mutation remains a subject of debate.

The guanine and cytosine nucleic acid bases have been studied experimentally and computationally, both as isolated molecules and in pairs. Gas-phase beam expansion studies of guanine have shown the presence of one enol and two keto tautomers,[4a,b] and partial assignments of the UV and IR spectra were performed with the aid of ab initio calculations. Similarly, resonant two-photon ionization (R2PI) experiments on cytosine indicated the presence of both keto and enol tautomers.[8] In contrast, R2PI studies of the guanine−cytosine (G···C) complex initially showed the presence of one structure with the cytosine in the enol form.[4e,f,9a] Additional measurements in the

* To whom correspondence should be addressed. E-mail: benny@fh.huji.ac.il.
† The Hebrew University of Jerusalem.
‡ University of California, Irvine.
§ Academy of Sciences of the Czech Republic and Center for Biomolecules and Complex Molecular Systems.
|| FOM Institute for Plasmaphysics Rijnhuizen.
⊥ University of California, Santa Barbara.

10.1021/jp051767m CCC: $30.25 
Published on Web 07/14/2005

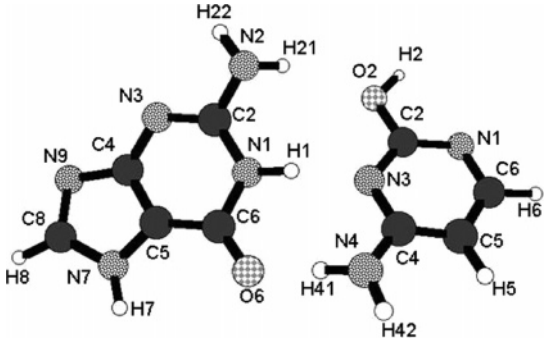


**Figure 1.** G···C enol geometry.

500−1800 $cm^{-1}$ range further showed that the G···C gas-phase complex contains guanine with a hydrogen atom attached to the N7 nitrogen (cf. Figure 1).[4c]

Theoretical calculations of the G···C complex have been performed for both hydrogen-bonded and stacked forms, at a variety of levels,[10] including the use of force fields, semiempirical methods, and ab initio methods. These calculations have shown the importance of the appropriate choice of basis set and type of calculation. The resolution of identity MP2 (RI-MP2) method yields better results than density functional theory (DFT), especially in the case of stacked pairs,[10] where DFT fails completely; the RI-MP2 method gives nearly the accuracy of MP2, at a fraction of the computational effort.[10h] The hydrogen-bonded Watson−Crick G···C complex was found to have a slightly nonplanar structure.[4c,10f] In contrast, the adenine−thymine Watson−Crick complex is found to be planar according to RI-MP2 calculations.[10c] Ab initio calculations have also shown that the Watson−Crick base pairs have a significant degree of flexibility,[10d] which may be an important contributing factor to the flexibility of DNA. Rare tautomeric forms (imino and enol forms) of the base pairs are present at very low levels in DNA (∼0.01%) and might play a significant role in mutagenic processes; these forms, as well as amino and keto forms, have also been studied computationally.[7,10i,j]

Vibrations of the base pairs are of particular interest due to their putative role in reactions such as proton transfer that may contribute to DNA mutation. Several vibrational frequency calculations have been performed in order to aid in structural assignments at the harmonic level.[4,10] Computational studies focusing on the intermolecular vibrational modes have also been performed, including analysis of the potential energy distribution in the modes,[11a] comparison with anharmonicity in other, planar base pairs,[11b] and inter-residue force assessment.[11c] However, the inclusion of anharmonicity is necessary for accurate calculations of torsional motions, including those which may be part of intermolecular modes; this is complicated by the fact that the G···C pair is nonplanar. Additionally, the inclusion of anharmonicity in the intermolecular mode calculations could aid in understanding the potential surfaces describing the proton transfer between the base pairs and, consequently, the feasibility of proposed proton transfer mechanisms. Recently, experiments were performed using pulsed IR spectroscopy in order to study the vibrational dynamics of both the A···U[12a] and G···C[12b] base pairs. Experimental information about the anharmonic coupling between modes was obtained but awaits more detailed understanding through theoretical anharmonic vibrational calculations. Above all, the availability of experimental spectroscopic data opens the way to testing and exploring the quality of available force fields. Needless to say, the anharmonic properties of the force fields are of central interest. For this purpose, spectroscopic calculations that incorporate the anharmonic effects are essential.

Fortunately, anharmonic frequency calculations have recently become easier to perform due to their inclusion in GAMESS,[13a−d] MOLPRO,[14] and GAUSSIAN.[15] The GAMESS and MOLPRO packages use vibrational self-consistent field (VSCF) theory and correlation-corrected VSCF (CC-VSCF) theory.[13c,d,14b] These methods, described in the Methods section in more detail, are based on assuming separability of the N-vibrational mode wave function. Together with the variational principle, this yields single mode equations that are solved self-consistently. The potential is truncated by including only single and double mode terms, and accuracy can be improved by including correlation effects (CC-VSCF). CC-VSCF anharmonic vibrational calculations have given large improvements over harmonic frequency calculations for biological molecules such as glycine,[16] a glycine−water complex,[17] and *N*-methylacetamide.[18] The GAUSSIAN program package contains an anharmonic vibrational calculation method developed by V. Barone.[15b] This method uses a second-order perturbation treatment based on quadratic, cubic, and semidiagonal quartic force constants; it has successfully been applied to molecules such as furan,[19] azabenzenes,[20] and uracil.[21]

While it is still too computer-costly to perform anharmonic vibrational calculations on molecules the size of the G···C complex with a completely ab initio potential surface, a recent improvement of the semiempirical PM3 method[13e,22] makes these calculations feasible, with a high level of accuracy. The suitability of PM3 is also shown by its successful application in reducing the computational time for CC-VSCF with ab initio surfaces; D. M. Benoit used preliminary PM3 computations in order to select relevant mode coupling terms.[23] Calculations of harmonic frequencies by empirical force fields also provide a computationally inexpensive alternative to ab initio calculations; however, they are not sufficiently accurate and are thus inadequate for use with anharmonic vibrational calculations.[16−18] In the present work, we present the results of RI-MP2/cc-pVDZ and RI-MP2/TZVPP ab initio calculations, and of anharmonic vibrational calculations, using adapted PM3 surfaces, and additional experimental data on the G···C enol complex, protonated at the 7-position. This paper is organized as follows: the methodology is presented in section II, the results and discussion are presented in section III, and conclusions and future work are given in section IV.

## II. Methods

**A. Ab Initio Calculations.** The G···C pair was optimized by gradient optimization at the RI-MP2 level using the DZ+P (cc-pVDZ [3s2p1d/2s1p]) and TZ+P (TZVPP [5s3p2d1f/3s2p1d]) basis sets, with a standard (default) auxiliary basis set.[10h,24−26] All ab initio calculations were carried out using the TURBOMOLE, version 5.6, program suite.[27] The harmonic frequencies calculated numerically at the RI-MP2/cc-pVDZ and RI-MP2/TZVPP levels of theory were both scaled by a universal factor of 0.956 to fit the experimental values of the N−H stretch modes of isolated guanine.[4e]

**B. Semiempirical Anharmonic Calculations.** Anharmonic vibrational calculations were performed using the VSCF and CC-VSCF methods included in the GAMESS[13] program package, with adapted PM3 surfaces.[22] The PM3 calculations were performed with an older version of MOPAC[13e] (which has been included in GAMESS), which does not have an amide molecular mechanics correction. Geometry optimization was performed using Cartesian coordinates. The VSCF method begins with the

Schrodinger equation in mass-weighted normal mode coordinates ($Q_1, \ldots, Q_N$)

$$\left[-\frac{1}{2}\sum_{j=1}^{N}\frac{\partial^2}{\partial Q_j^2} + V(Q_1, \ldots, Q_N)\right]\Psi_n(Q_1, \ldots, Q_N) = E_n\Psi_n(Q_1, \ldots, Q_N) \quad (1)$$

for potential function $V$, number of modes $N$, and state $n$. Together with the ansatz

$$\Psi^{(n)}(Q_1, \ldots, Q_N) = \prod_{j=1}^{N}\psi_j^{(n)}(Q_j) \quad (2)$$

and the variational principle, single mode eqs 3 and 4 are obtained, where $\bar{V}_j^{(n)}$ is the effective potential. Equations 3 and 4 are solved self-consistently.

$$\left[-\frac{1}{2}\frac{\partial^2}{\partial Q_j^2} + \bar{V}_j^{(n)}(Q_j)\right]\psi_j^{(n)}(Q_j) = \epsilon_j^{(n)}\psi_j^{(n)}(Q_j) \quad (3)$$

$$\bar{V}_j^{(n)}(Q_j) = \langle\prod_{l\neq j}^{N}\psi_l^{(n)}(Q_l)|V(Q_1, \ldots, Q_N)|\prod_{l\neq j}^{N}\psi_l^{(n)}(Q_l)\rangle \quad (4)$$

The computational effort is reduced by assuming that the potential of the system can be represented as a sum of single mode ($V_j^{\mathrm{diag}}(Q_j)$) and pair-coupling ($V_{ij}^{\mathrm{coup}}(Q_i, Q_j)$) terms

$$V(Q_1, \ldots, Q_N) = \sum_{j=1}^{N}V_j^{\mathrm{diag}}(Q_j) + \sum_{i}^{N}\sum_{i<j}^{N}V_{ij}^{\mathrm{coup}}(Q_i, Q_j) \quad (5)$$

The diagonal and coupling terms of the potential are computed using grid techniques along the single mode and double mode coordinates and

$$V_{ij}^{\mathrm{coup}}(Q_i, Q_j) = V(0, \ldots, Q_i, \ldots, Q_j, \ldots, 0) - V_i^{\mathrm{diag}}(Q_i) - V_j^{\mathrm{diag}}(Q_j) \quad (6)$$

The potential surfaces used for vibrational self-consistent field (VSCF) calculations were adapted by shortening or lengthening the normal coordinates of standard PM3 surfaces, so that the harmonic adapted PM3 frequencies would be equivalent to the ab initio ones. Thus,

$$V_{\mathrm{PM3}}^{\mathrm{new}}(Q_i) = V_{\mathrm{PM3}}^{\mathrm{standard}}(\lambda_i Q_i) \quad (7)$$

for each normal coordinate ($Q_i$) and where each $\lambda_i$ is calculated by using the ratio of the unscaled ab initio and standard PM3 harmonic frequencies:

$$\lambda_i = \omega_i^{\mathrm{RI\text{-}MP2}}/\omega_i^{\mathrm{PM3}} \quad (8)$$

The normal modes at the two levels of calculation (ab initio and standard PM3) were compared by inspection of their dot products and visual inspection with the MOLDEN[28] and MacMolPlt[29] graphics programs. (The normal mode description may differ at the various levels of computation; e.g., the RI-MP2/DZ+P $NH_2$ symmetric stretch on cytosine contains a small percentage of hydrogen-bonded NH stretch on guanine, whereas for PM3 it is the $NH_2$ asymmetric stretch that contains very slight motion of the hydrogen-bonded NH group on guanine.) All modes were scaled in the present calculation, and the results of the RI-MP2/DZ+P ab initio calculation were used for the scaling. Sixteen grid points were used for each normal mode coordinate, and the SCF convergence factor for PM3 energy calculations was $1 \times 10^{-6}$. (The choice of coordinates for the problematic torsional modes may affect the value of the coupling potential, as discussed below.) For further information about the coordinate scaling, the reader is referred to ref 22.

**C. Experimental Section.** The experiments were performed in two almost identical and previously described molecular beam setups, one in Santa Barbara,[30] covering the near-IR region, and a second at FELIX,[31] covering the mid-IR region. We applied a mixture of solid guanine and cytosine crystals and graphite powder to the surface of a solid graphite bar, placed directly under the orifice of a pulsed valve.

Directly after opening the nozzle, a pulsed Nd:YAG laser, at 1064 nm, <1 mJ/pulse, desorbs sample molecules from the graphite matrix. The desorbed molecules are entrained in the supersonically expanding carrier gas. In the adiabatic expansion, the internal degrees of freedom in the nucleobase molecules are cooled to about 10 K. The expansion conditions enable the formation of clusters of guanine and cytosine, which are internally cooled as well.

To obtain R2PI spectra, we use a tunable dye laser in the region from 264 to 268 nm. By monitoring the mass peak of the GC cluster while varying the two-photon ionization wavelength, we obtain the mass selected excitation spectra. We record UV−UV double resonance spectra by applying a delay of about 200 ns between dye laser pulses. The laser that fires first serves as an intense "burn" laser and is scanned over the R2PI spectrum region, while the delayed laser serves as the "probe" laser, fixed on one resonance. When both lasers are tuned to a resonance of the same conformer, a decrease in the signal of the probe laser results. With this technique, we can determine the origins and the number of cluster structures. To obtain the IR spectrum for a specific GC structure, we use IR−UV double resonance spectroscopy, in which an IR laser functions as the burn laser pulse. The UV laser is tuned to a resonance of the specific GC structure, while we scan the IR laser. When the IR laser is resonant with a vibrational transition that belongs to the same cluster, it causes a depletion of the ground state, which leads to a decrease in the intensity of the ion signal. Thus, we produce structure selected as well as mass selected IR spectra.

The near-IR radiation is produced by an OPO system (Laser Vision) pumped by a Nd:YAG laser (Quanta-Ray) operated at its fundamental wavelength of 1064 nm. For this work, we operated in the range 3200−3700 $cm^{-1}$, which encompasses NH, $NH_2$, and OH stretching modes. The output of the OPO system is 8 mJ/pulse, and the bandwidth is 3 $cm^{-1}$.

The mid-IR radiation is produced at the Free Electron Laser for Infrared eXperiments (FELIX) user facility at the FOM Institute for Plasma Physics in Rijnhuizen, The Netherlands.[31b] The temporal output of this 10 Hz, pulsed laser system consists of long bursts (macropulses) of micropulses. The micropulse spacing within the burst is set to 1 ns. The spectral bandwidth is adjusted to approximately 0.5% (fwhm) of the central frequency which corresponds to a micropulse duration of about 100 optical cycles. We used a frequency range from 500 to 2000 $cm^{-1}$. Typically, energies of up to 100 mJ can be reached in the macropulse.

## III. Results and Discussion

**A. Geometries.** The G···C complex is illustrated in Figure 1. This is one of three GC structures found in our laser desorption jet cooling experiments. It is triply hydrogen bonded with cytosine in the enol form, and it is the third most stable

**TABLE 1: G···C Enol Geometries: Inter-ring Parameters and Parameters with the Largest Deviations (Distances in Angstroms and Angles in Degrees)**

| parameter | atoms (base) | PM3 | RI-MP2/cc-pVDZ | RI-MP2/TZVPP |
|---|---|---|---|---|
| bond distance | C5−N7 (G) | 1.405 | 1.371 | 1.364 |
| | N1−C2 (G) | 1.422 | 1.387 | 1.377 |
| | C6−N1 (G) | 1.424 | 1.394 | 1.384 |
| | N2−C2 (G) | 1.419 | 1.384 | 1.370 |
| | C4−N4 (C) | 1.389 | 1.353 | 1.343 |
| | C2−N1 (C) | 1.368 | 1.333 | 1.321 |
| | N3−C2 (C) | 1.364 | 1.338 | 1.327 |
| H-bond distance | O2(C)−H21(G) | 2.477 | 2.091 | 2.073 |
| | N3(C)−H1(G) | 1.829 | 1.921 | 1.907 |
| | H41(C)−O6(G) | 1.806 | 1.821 | 1.796 |
| bond angle | C6−N1−C2 (G) | 120.541 | 125.190 | 125.005 |
| | O2−C2−N1 (C) | 119.864 | 116.419 | 116.727 |
| | H2−O2−C2 (C) | 108.965 | 104.208 | 105.180 |
| | H42−N4−C4 (C) | 113.796 | 117.639 | 118.619 |
| | H1−N1−C6 (G) | 119.000 | 115.730 | 115.963 |
| | H21−N2−C2 (G) | 113.836 | 115.550 | 117.693 |
| | H22−N2−C2 (G) | 113.424 | 110.492 | 112.566 |
| dihedral angle | N2−C2−N1−C6 (C) | 170.674 | 175.512 | 176.062 |
| | C6−C5−C4−N4 (C) | −175.061 | −178.541 | −179.308 |
| | H41−N4−C4−C5 (C) | −159.703 | −165.709 | −169.543 |
| | H42−N4−C4−C5 (C) | −22.245 | −13.403 | −7.774 |
| | H1−N1−C6−C5 (G) | −174.932 | −177.708 | −179.174 |
| | H21−N2−C2−N1 (G) | 39.825 | 34.851 | 28.688 |
| | H22−N2−C2−N1 (G) | 169.696 | 165.027 | 166.742 |
| amide dihedral | H1−N1−C6−O6 (C) | 5.122 | 2.600 | 1.065 |
| interring dihedral | N4(C)−O6(G)−C6(G)−C5(G) | −161.151 | −167.729 | −163.286 |
| | C4(C)−N4(C)−O6(G)−C6(G) | −54.235 | −34.022 | −34.157 |
| | N3(C)−C2(C)−N1(C)−N2(G) | −131.310 | −143.365 | −138.174 |
| | C2(G)−N2(G)−O2(C)−C2(C) | −56.692 | −48.257 | −46.926 |
| | C2(G)−N1(G)−N3(C)−C4(C) | 157.577 | 161.977 | 157.452 |
| | C4(C)−N3(C)−C2(C)−N1(G) | 177.338 | −176.935 | −172.657 |

structure, according to energies calculated at the RI-MP2/TZVPP level.[32] We have chosen this structure for the current analysis because it is the one for which we have obtained the most complete set of experimental vibrational frequencies, including the lower frequencies below 3000 $cm^{-1}$. Table 1 contains some of the geometric information obtained at the three computational levels used in the present work. While most of the bond distances are within 0.04 Å for all levels of calculation, the bonds whose distances have the largest deviations are given in Table 1. They are all CN bond distances, primarily associated with the hydrogen-bonding portions of the guanine and cytosine rings. Hydrogen-bond distances are generally similar at all three levels, with the exception of the O2(C)−H21(G) bond, differing by 0.4 Å between the PM3 and RI-MP2/TZVPP results. In contrast, the H41(C)−O6(G) hydrogen-bond distance calculated by PM3 is closer to the RI-MP2/TZVPP result than the RI-MP2/cc-pVDZ result. Difficulties with the use of PM3 for describing hydrogen-bonded complexes have been discussed by several authors (see, for example, refs 33 and 34). Harb et al.[33] found that the depth of the potential wells in hydrated systems and the positions of the minima, described by PM3, are in error; they were correctable by the use of a core−core interaction term which was obtained by fitting with MP2/aug-cc-pVQZ data. In the present complex, this is reflected in a low value for the complex binding energy (−6.8 kcal/mol without ring deformation and −8.5 kcal/mol with ring deformation, basis set superposition error not included).

The PM3 bond angles are generally in agreement with the ab initio data, while, once again, the angles with the largest deviations are primarily adjacent to the CN bonds, along the hydrogen-bonded portions of the rings. Some of the PM3 bond angles are closer to the cc-pVDZ results, while others are closer to the TZVPP data. Dihedral angle differences are largest for the amino group pyramidization and the angle of the amino group with the ring. The PM3 pyramidization is greater than that of the ab initio methods, and the RI-MP2/cc-pVDZ data reflect more pyramidization than the RI-MP2/TZVPP results. Force fields such as AMBER and CHARMM[10a] predict planarity of the amino group.

The guanine "amide dihedral" (NH−C═O angle) is less planar in PM3 than with the ab initio methods. Later versions of PM3 in the MOPAC[13e] package correct this angle using molecular mechanics; however, it appears that, in consideration of the problems described with the use of force fields for the present system, the use of the PM3 molecular mechanics correction is undesirable.

The improper dihedral angles indicating the angles between the guanine and cytosine rings generally differ at all levels of calculation. Half of the PM3 inter-ring angles are closer to the RI-MP2/TZVPP results. The largest discrepancy is in the angle between the cytosine $NH_2$ group and the C═O group of the guanine ring. This may be attributable to the greater $sp^3$ character of the $NH_2$ group, calculated by PM3. Overall, while PM3 does not exactly replicate the ab initio results, it yields a good workable structure.

**B. Frequencies.** Frequency data, both experimental and theoretical, are presented in Table 2 and in Figure 2. (Each mode is described according to the common feature at the different levels of calculation.) The results of CC-VSCF calculations, using the adapted PM3 potential and unscaled RI-MP2/cc-pVDZ harmonic frequencies are provided, in addition to the results of multiplication of the RI-MP2/cc-pVDZ and RI-MP2/TZVPP data by a universal scaling factor of 0.956. This scaling factor is used in order to correct the harmonic frequencies for anharmonicity effects. The average percentage deviations for these calculations are presented in Table 3, and Figure 3 provides percentage deviations for a sample of modes.

In consideration of the frequency data presented in Table 2 and in Figure 2, it is clear that, in general, the frequency data show good agreement with experiment for all three methods (CC-VSCF with adapted PM3 and scaled RI-MP2/cc-pVDZ and RI-MP2/TZVPP). However, a definite assignment of all peaks is difficult, due to their number and the lack of isotopic substitution data. For the stretching modes (∼2900−3700 $cm^{-1}$),

**TABLE 2: Vibrational Frequencies, Calculated and Measured (Modes Are in the Order Given by PM3 Calculations)**

| exptl value | | harm. RI-MP2 | | scaled PM3 | scaled RI-MP2 harmonic[p] | |
|---|---|---|---|---|---|---|
| ref 32/note | refs 4c,e | cc-pVDZ | description | CC-VSCF | TZVPP | cc-pVDZ |
| 3617 | 3603 | 3783 | OH str | 3534 | 3623 | 3617 |
| 3439 | 3426 | 3551 | $NH_2$ sym str G | 3294 | 3407 | 3395 |
| 3094 | | 3336 | $NH_2$ sym str[q] | 3081 | 3157 | 3189 |
| 3564 | 3552 | 3672 | NH str G, no H-bond | 3452 | 3514 | 3510 |
| 3545 | 3532 | 3686 | $NH_2$ asym str G | 3393 | 3541 | 3524 |
| 3525 | 3510 | 3710 | $NH_2$ asym str[q] | 3338 | 3558 | 3547 |
| 3120 | | 3258 | CH str C | 3063 | 3109 | 3115 |
| 3139 | | 3294 | CH str G | 3125 | 3147 | 3149 |
| 2975[b] | | 3220 | CH str C | 3026 | 3075 | 3078 |
| 3002[a] | | 3245 | NH str G, H-bonded | 2829 | 3072 | 3102 |
| | 1706 | 1803 | C═O str | 1773 | 1691 | 1724 |
| | 1639 | 1720 | ring str | 1689 | 1633 | 1644 |
| *c* | 1582 | 1595 | CC str G | 1564 | 1509 | 1525 |
| | 1558 | 1634 | CN, CC str C | 1602 | 1546 | 1562 |
| *c* | 1582 | 1650 | $NH_2$ b G | 1585 | 1583 | 1577 |
| | 1662 | 1704 | $NH_2$ b C,G, CN str G[q] | 1656 | 1620 | 1629 |
| | 1624 | 1675 | $NH_2$ b C | 1615 | 1597 | 1601 |
| *c* | 1515 | 1588 | CN str, $NH_2$ b G[q] | 1548 | 1506 | 1518 |
| | 1441 | 1488 | C─O(H) str | 1458 | 1411 | 1423 |
| *c* | 1515 | 1563 | CN str C | 1535 | 1484 | 1494 |
| | 1462 | 1508 | CN str G | 1487 | 1425 | 1442 |
| | 1394 | 1416 | NH inpb G, no H-bond | 1378 | 1351 | 1354 |
| | 1429 | 1447 | CC str, $NH_2$ b C | 1431 | 1374 | 1383 |
| *c* | 1515 | 1542 | CN str, NH inpb G | 1510 | 1459 | 1474 |
| | 1374 | 1421 | ring str, NH b G | 1394 | 1342 | 1358 |
| | 1401 | 1392 | CN str, NH b G, H-bond | 1363 | 1325 | 1331 |
| | 1269 | 1261 | COH b | 1232 | 1202 | 1206 |
| | 1269 | 1319 | CC str G | 1288 | 1256 | 1261 |
| *d* | 1330 | 1373 | CH b, ring mode C | 1358 | 1307 | 1313 |
| | 1199 | 1241 | ring str, NH b G | 1215 | 1185 | 1186 |
| *e* | 1071 | 1087 | NH b G, no H-bond | 1056 | 1043 | 1039 |
| | 1330 | 1332 | COH b, NCH b C | 1330 | 1267 | 1273 |
| *e* | 1071 | 1115 | CH b C | 1090 | 1062 | 1066 |
| *e* | 1129 | 1140 | $NH_2$ wag G | 1128 | 1084 | 1090 |
| *f* | 1000 | 1005 | ring mode C | 994 | 962 | 961 |
| *e* | 1129 | 1146 | $NH_2$ wag, CH b C | 1138 | 1092 | 1096 |
| *f* | 1071 | 1057 | $NH_2$ wag, CN str G | 1049 | 1009 | 1010 |
| | 1152 | 1182 | CH b G | 1171 | 1124 | 1130 |
| | 1000 | 1033 | CH b C | 1027 | 982 | 988 |
| *f* | 941 | 984 | CH b oop C | 982 | 943 | 941 |
| *f* | 928 | 951 | NCN inpb G | 944 | 911 | 909 |
| | 705 | 725 | $NH_2$ oopb G | 713 | 695 | 693 |
| *h* | 818 | 820 | CH oopb, ring tors C | 821 | 796 | 784 |
| *i* | 818 | 821 | CH oopb G | 826 | 798 | 785 |
| *j* | 785 | 794 | ring mode C | 796 | 760 | 759 |
| *h* | 845 | 835 | CNC b, shear G | 829 | 799 | 798 |
| | 740 | 743 | $NH_2$ oopb, shear C[q] | 728 | 718 | 710 |
| | 785 | 758 | CCC oopb G | 759 | 739 | 725 |
| | 785 | 778 | NH oopb G,ring tors C | 788 | 757 | 744 |
| *g* | 965 | 891 | NH oopb, G, H-bond | 905 | 856 | 852 |
| *m* | 629 | 644 | ring shear G[q] | 635 | 612 | 616 |
| | 675 | 681 | ring mode G | 667 | 655 | 651 |
| *f* | 705 | 708 | ring tors G | 713 | 683 | 677 |
| *f* | 705 | 703 | ring tors C | 710 | 681 | 672 |
| | 559 | 559 | ring shear C | 553 | 538 | 534 |
| *k* | 606 | 625 | NCN oopb G | 650 | 548 | 598 |
| | not seen | 602 | ring shear C | 597 | 577 | 576 |
| *l* | 629 | 653 | NH, CH oopb, tors G | 648 | 626 | 624 |
| | 538 | 541 | ring shear G | 535 | 521 | 517 |
| *f* | 514 | 493 | shear G, C | 491 | 473 | 471 |
| | not seen | 410 | NH oopb G ($NH_2$ tors) | 464 | 384 | 392 |
| *f* | 538 | 518 | shear C,G[q] | 533 | 499 | 495 |
| *n,o* | 514 | 532 | COH tors | 570 | 506 | 509 |
| *n* | not seen | 461 | ring tors C | 481 | 444 | 441 |
| *n* | 514 | 499 | NH oopb G | 581 | 488 | 477 |
| | not seen | 321 | NCC═O shear G | 336 | 311 | 307 |
| | not seen | 373 | ring tors G | 385 | 356 | 356 |
| | not seen | 355 | $NH_2$ wag G | 355 | 342 | 340 |
| | not seen | 377 | $NH_2$, OH wag C | 381 | 366 | 361 |
| *n* | not seen | 432 | $NH_2$ group tors G | 576 | 439 | 413 |

**TABLE 2: (Continued)**

| exptl value | | harm. RI-MP2 | | scaled PM3 | scaled RI-MP2 harmonic[p] | |
|---|---|---|---|---|---|---|
| ref 32/note | refs 4c,e | cc-pVDZ | description | CC-VSCF | TZVPP | cc-pVDZ |
| | not seen | 227 | ring tors C | 234 | 218 | 217 |
| | not seen | 195 | ring tors C[q] | 204 | 186 | 186 |
| | not seen | 208 | ring tors G | 228 | 202 | 198 |
| | not seen | 120 | inter-ring str[q] | 132 | 120 | 115 |
| | not seen | 171 | ring tors G | 191 | 165 | 164 |
| | not seen | 150 | ring tors G | 158 | 144 | 144 |
| | not seen | 110 | inter-ring opening | 116 | 107 | 105 |
| | not seen | 85 | inter-ring shearing | 89 | 80 | 81 |
| | not seen | 63 | inter-ring stagger | 88 | 58 | 60 |
| *n* | not seen | 37 | inter-ring propeller | 66 | 36 | 35 |
| *n* | not seen | 24 | inter-ring buckle | 68 | 26 | 23 |

[a] The line calculated to be at 2829 $cm^{-1}$ may be off of the experimental figure. [b] The line calculated to be at 3026 $cm^{-1}$ may overlap with the experimental 3002 or 3094 $cm^{-1}$ lines. [c] Apparently, there are several overlapping peaks at 1558 and 1515 $cm^{-1}$, and therefore, a definite assignment of the weak lines calculated at 1587, 1564, and 1548 $cm^{-1}$ is difficult. [d] A line at 1359 $cm^{-1}$ may be experimental noise rather than a peak. [e] There appear to be several overlapping lines at 1129 and 1071 $cm^{-1}$. [f] May be too weak to be detected, overlaps with other peaks, or indistiguishable from experimental noise. [g] This mode has large diagonal and coupling anharmonicity effects; it may be at 845 $cm^{-1}$. [h] Intensity data indicate that the assignments of these lines may actually be reversed. [i] May overlap with line at 845 $cm^{-1}$ instead. [j] May overlap with line at 818 $cm^{-1}$ instead or may not be seen. [k] Based on intensity; line may actually be at 675 $cm^{-1}$. 606 $cm^{-1}$ is not listed in ref 4c, seen in figure. [l] May overlap with peak at 675 $cm^{-1}$ instead. [m] May overlap with peak at 606 $cm^{-1}$ instead. [n] This mode has large diagonal anharmonicity and may require a different type of calculation. [o] May overlap with other peaks in the 500−600 $cm^{-1}$ range instead. [p] RI-MP2 harmonics were scaled by 0.956. [q] Indicates weaker correspondence between ab initio and PM3 modes.

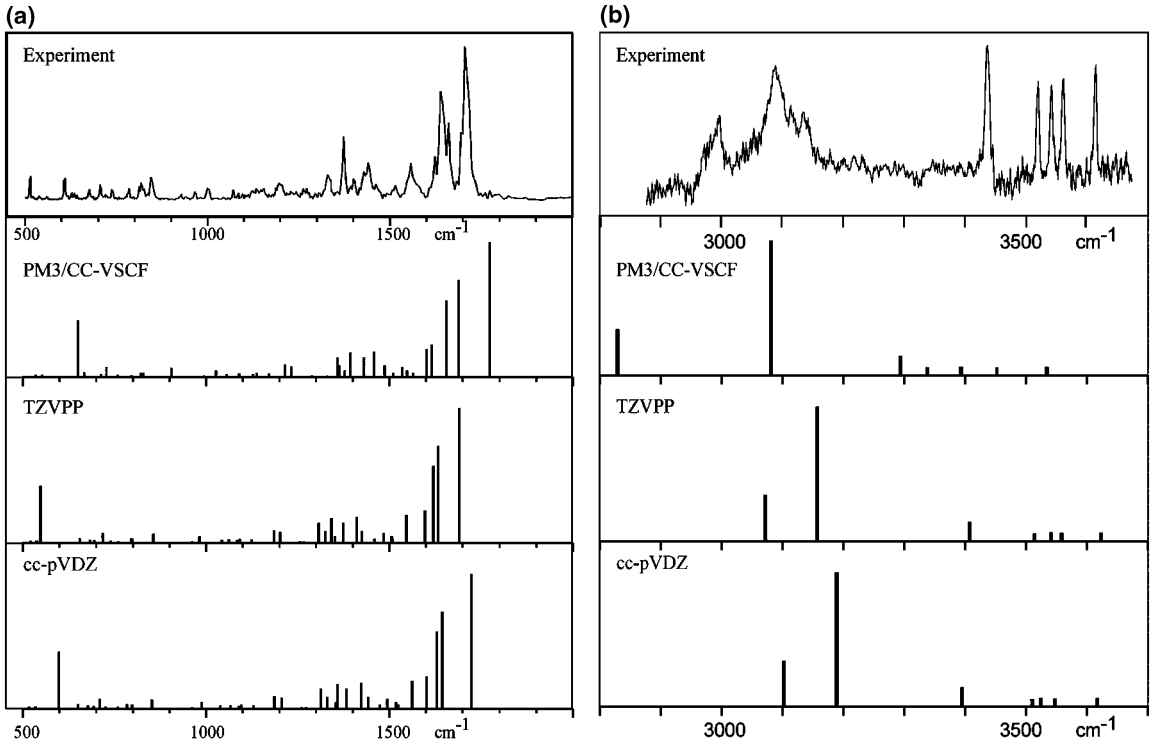


**Figure 2.** Comparison of experimental data with calculations, as indicated (for CC-VSCF results, ab initio intensities were used because this portion of the VSCF calculation has not yet been adapted; experimental data also appear in refs 4c and 32).

**TABLE 3: Percentage Deviations of Frequency Data (Average of Absolute Values)**

| | CC-VSCF | RI-MP2 unscaled | | RI-MP2 scaled | |
|---|---|---|---|---|---|
| | PM3 adapted | cc-pVDZ | TZVPP | cc-pVDZ | TZVPP |
| assigned modes | 2.27 | 2.63 | 2.50 | 2.90 | 3.00 |
| stretches only | 3.56 | 4.63 | 4.55 | 0.80 | 0.78 |

there is a clear advantage to the use of the RI-MP2 method with the use of an empirical scaling factor, used in order to account for anharmonicity, which is multiplied by the harmonic frequencies. However, since the scaling factor is empirical, it does not provide information about the potential surface. In addition, each ab initio harmonic computational method requires its own scaling factor. Inclusion of anharmonic effects also can change the frequency ordering of the modes. The percentage deviation, when all modes are included, is slightly better for the CC-VSCF calculation than for the empirically scaled ab initio harmonic calculations. It is expected that the use of a PM3 surface that is adapted to the TZVPP basis calculations would give a better percentage deviation. Surprisingly enough, the universal scaling factor used with the RI-MP2 calculations actually seems to reduce the accuracy of the results for the nonstretching modes. Since the 0.956 factor was obtained from fitting of NH stretches in the 3000−3500 $cm^{-1}$ range, it is possible that a more suitable scaling factor could be obtained

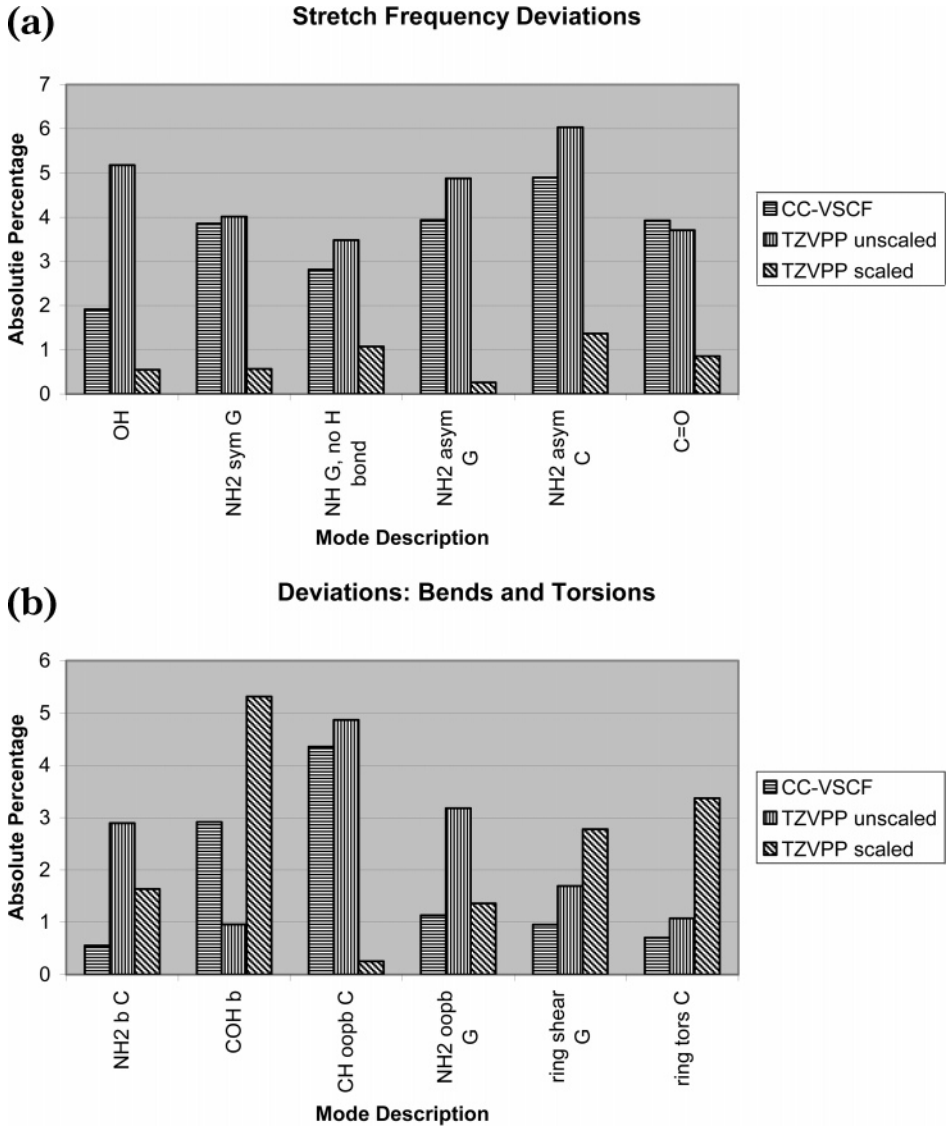


**Figure 3.** Percentage deviations from experiment of (a) stretching and (b) bending and torsion frequencies.

by fitting a data set that includes stretches, bends, and torsions. In another work devoted to comparison of the calculated MP2 and experimental spectra of guanine and guanosine, Nir et al.[9a] scaled the frequencies with a factor of 0.942 for OH stretches and 0.951 for NH stretching vibrations, based on a comparison with an experimental *para*-aminophenol IR double resonance spectrum.[9b] Apparently, the use of universal scaling factors for ab initio harmonic frequency calculations should be re-examined (or there could be errors in the present assignments).

**C. Anharmonicity.** The G···C enol complex has a total of 81 modes, six of which are soft intermolecular modes. The six intermolecular modes can be described (according to the terminology used for interbase rotations[35]) as stretch, stagger, shearing, opening, propeller, and buckle. As described above, the advantage of using the anharmonic VSCF and CC-VSCF procedures is that they give insight into the nature of the potential surface. Table 4 shows a sampling of the amount of anharmonicity in various types of modes. The individual anharmonicities were calculated according to

$$\text{intrinsic anharmonicity \%} = (v_{\text{diagonal}} - v_{\text{harmonic}})100/v_{\text{CC-VSCF}} \quad (9)$$

and

$$\text{coupling anharmonicity \%} = (v_{\text{CC-VSCF}} - v_{\text{diagonal}})100/v_{\text{CC-VSCF}} \quad (10)$$

where "diagonal" or "intrinsic" refers to the anharmonicity along a single mode, without the inclusion of coupling. Table 4 lists the typical range of anharmonicities, that is, the range of the average minus/plus the standard deviation.

In general, the tabulated results indicate that, as expected, the type of anharmonicity depends on the nature of the vibrational mode. For the hydrogenic stretching modes, the intrinsic anharmonicity tends to be more significant than the anharmonicity due to mode coupling. The main exceptions are the $NH_2$ asymmetric stretches for both guanine and cytosine. A sample of integrated couplings between a variety of modes and the $NH_2$ asymmetric stretch of guanine is given in Figure 4 (note that the *y*-axis is logarithmic). These couplings are an approximation of the integration

$$I = \langle \psi_i(Q_i)\, \psi_j(Q_j) | V_{ij}(Q_i, Q_j) | \psi_i(Q_i)\, \psi_j(Q_j) \rangle \quad (11)$$

where $Q_i$ and $Q_j$ are the normal mode coordinates for modes *i*

**TABLE 4: Intrinsic and Coupling Anharmonicities**

| description | value | intrinsic | coupling[d] |
|---|---|---|---|
| hydrogenic stretches | typical[a] | 2−6.8% | 1−6.4% |
| | high | NH str (G, H-bonded), 10% | $NH_2$ asym str (G), 8.9% |
| | | | $NH_2$ asym str (C), 7.5% |
| | low | $NH_2$ asym str (G), 0.5% | NH str (G, no H-bond), 0.9% |
| C═O stretch | | 0.20% | 1.50% |
| bends 1000−1700 $cm^{-1}$ | typical[a] | 0−1.2% | 1.3−3.1% |
| | high | CH b (G), 3.1% | NH b (G, no H-bond), 3.9% |
| | | NH b (G, no H-bond), 1.8% | CH b (G), 3.7% |
| | low | - | COH b, NCH b C 0.8% |
| oop bends, shear, torsion[b] | typical[a] | 0−4.2% | 0.30−4.2% |
| | high | NH oopb (G, H-bond), 10.5% | NH oopb (G, H-bond), 7.4% |
| | | CH oopb (G), 7.5% | CH oopb (G), 5.6% |
| | low | | CCC oopb (G), 0% |
| intermolecular modes | range[c] | 0−11.2% | 0.4−24.7% |

[a] Range of average plus/minus standard sample deviation. [b] Sample excludes modes for which Cartesian coordinates are not preferred. [c] Sample is small and excludes the "buckle" mode, due to coordinates. [d] Actual percentages may be slightly greater because the VSCF frequency calculation scaled down some of the coupling potential points in order to obtain convergence (smallest factor = 0.73).

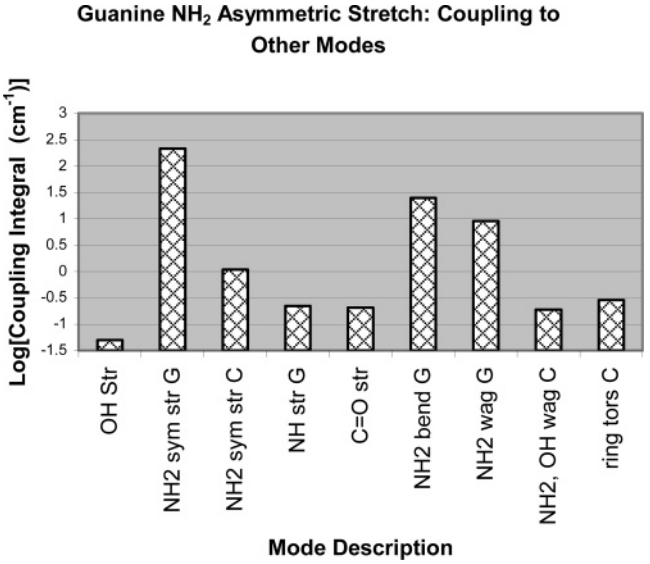


**Figure 4.** Integrated coupling of a variety of modes with the $NH_2$ asymmetric stretch of guanine (logarithmic scale).

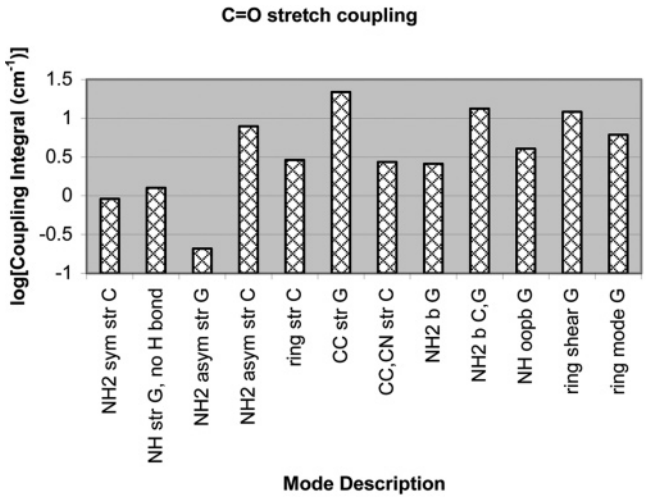


**Figure 5.** Integrated coupling of a variety of modes with the C═O stretch (logarithmic scale).

and *j*. This was computed by using the sum

$$I \simeq \sum_{m,n} |\psi_i(Q_{i,m})|^2 |V_{ij}(Q_{i,m}, Q_{j,n})| |\psi_j(Q_{j,n})|^2 \, dQ_i \, dQ_j \quad (12)$$

where *n* and *m* indicate points on the computational grid and psi is the ground state wave function. For this mode, there is greater coupling to modes located nearest to the same $NH_2$ group (this topic is discussed further below).

As shown in Table 4, the C═O stretch has relatively low anharmonicity, as anticipated, due to its double bond character. Most of the anharmonicity for this mode also arises from coupling, and again, the strongest contributing factor appears to be mode location (see Figure 5).

The bending modes in the range 1000−1700 $cm^{-1}$ are typified by a lower intrinsic anharmonicity, with a more significant contribution from coupling. The modes with the largest anharmonicity, both intrinsic and coupling, are the CH and NH in-plane bends (wags) of the five-membered ring in guanine. The lowest anharmonicity is in a mode containing the COH bend, together with the NCH in-plane bend of cytosine. The out-of-plane bends, shearing and torsional modes, below ∼1000 $cm^{-1}$, have comparable ranges of intrinsic and coupling anharmonicity; certainly the specific percentages depend on the mode in question. This is in contrast to the common assumption that the lower frequency bends and torsions show a higher degree of coupling. While it appears that this assumption is not necessarily true, the coupling potential could change with the use of a different force field. For the average of the anharmonicities and the inter-ring mode average, modes showing a large percentage of intrinsic anharmonicity (∼15% or more) were omitted. Such high anharmonicities are commonly an indication that a different coordinate system would be more suitable for the VSCF calculation.[36] The percentages of anharmonicity due to coupling are greater than the intrinsic anharmonicity, for all of the inter-ring modes.

Table 5 lists the modes whose coupling is the largest, according to the integration given in eq 12. The coupling potentials of modes for which the VSCF procedure is expected to work better in a different coordinate system are not included in the table where the headings "coordinates suitable" are given. In order to understand the factors contributing to significant coupling, the integrated coupling for a sampling of nine modes was plotted against a number of variables (for the coupled mode) including the force constant, reduced mass, inverse of the square root of the reduced mass ($1/\sqrt{\mu}$), dot product of the absolute values of the normal mode vectors, and product of the squares of thenormal mode coefficients (this would be greater than the dot product for modes in orthogonal directions). There is a correspondence for three of the modes studied, between the coupling of the modes considered and the square of the normal

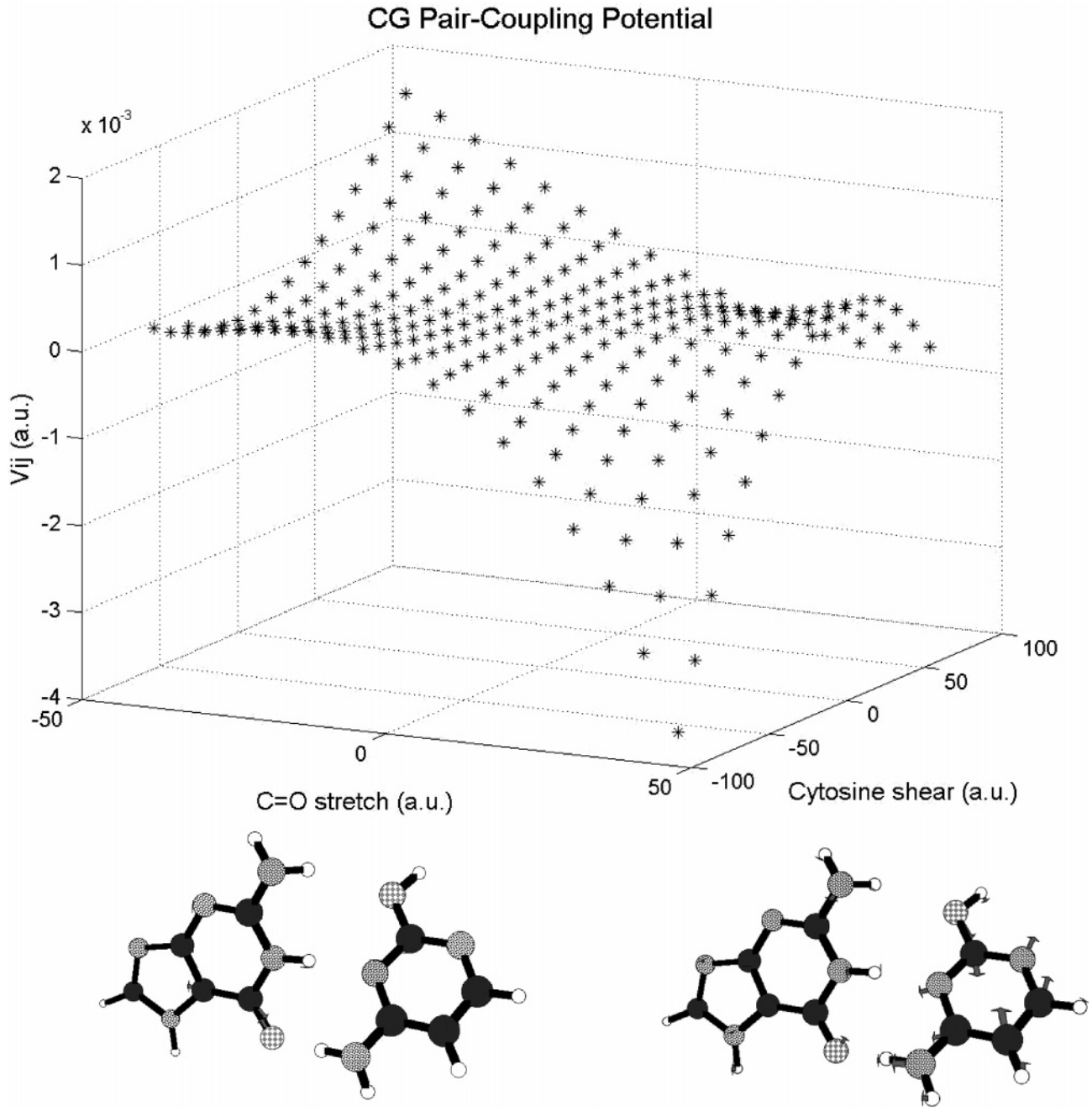


**Figure 6.** Coupling potential for the C═O stretch and cytosine ring shearing modes.

**TABLE 5: Strong Mode−Mode Couplings**

| mode type | mode 1 | mode 2 |
|---|---|---|
| all | $NH_2$ sym str (G) | $NH_2$ group tors (G) |
| | OH str | COH tors |
| | NH str (no H-bond, G) | NH oopb (no H-bond, G) |
| all, | $NH_2$ sym str (G) | $NH_2$ asym str (G) |
| coordinates suitable | NH str (H-bonded, G) | NH oopb, (H-bonded, G) |
| | $NH_2$ sym str (C) | shear (G, C) |
| all inter-ring | $NH_2$ group tors (G) | buckle |
| | COH tors | stagger |
| | $NH_2$ group tors (G) | inter-ring str |
| inter-ring, | NH str (H-bonded, G) | opening |
| coordinates suitable | shear (G, C) | stagger |
| | $NH_2$ asym str (C) | inter-ring str |

mode coefficients; these modes are the OH stretch ($r^2 = 0.81$), the $NH_2$ asymmetric stretch of guanine ($r^2 = 0.63$), and the $NH_2$ bend of cytosine ($r^2 = 0.59$). The other modes showed weaker correlations to the variables, if any. For three intermolecular modes that were studied, the strongest correlation was with $1/\sqrt{\mu}$; however, this was so low that it may be negligible ($r^2 = 0.11-0.17$). In general, although the sample is small, it can be concluded that there is not only one contributing factor to the mode coupling. The location of the coupled modes influences some of the mode couplings, but it appears that for a large percentage of the modes other factors are significant (these may include, for example, dipolar forces). It is also of experimental and theoretical interest that there is the possibility of strong coupling between stretching modes and intermolecular modes. Generally, the largest coupling integrals for the intermolecular modes were an order of magnitude lower than those of the stretching modes (the largest is 11 $cm^{-1}$ for coupling of the hydrogen-bonded NH stretch of guanine with the "opening" mode; the magnitude of the coupling could change with the use of a different potential).

The mode primarily described as the hydrogen-bonded NH stretch on guanine has an unusually high intrinsic anharmonicity for a hydrogenic stretch and an average coupling anharmonicity (see Table 4). An analogous mode for the adenine−uracil system was studied by Woutersen and Cristalli[12a] and was found to play a significant role in vibrational relaxation through energy transfer to hydrogen-bonded modes. This is consistent with the result given in Table 5, showing strong coupling between the hydrogen-bonded NH stretch of guanine and the inter-ring opening mode, and with the strong coupling that was also calculated for the inter-ring "stretch" mode, not listed in the table. Figure 6 shows the coupling potential between the C═O stretch and one of the cytosine shearing modes (frequency of 597 $cm^{-1}$ calculated with CC-VSCF). This coupling is of interest in relation to the 2D-IR experiments on oligonucleotides that were performed by Krummel et al.,[12b] indicating that ring vibrations of the bases are coupled to the carbonyl stretches. For the modes shown in Figure 6, the total coupling integral (of eq 12) over the ground state wave functions is 1.7 $cm^{-1}$. Since higher vibrational states sample the potential surface further away from equilibrium, it is likely that the coupling in excited vibrational states would be stronger.

## IV. Conclusions and Future Work

The present work has shown that the CC-VSCF method, with adapted PM3 potential surfaces, is useful in obtaining accurate frequency information for biological molecules. While high-quality ab initio calculations offer good accuracy (when empirical scaling factors are applied to the harmonic frequencies), the anharmonic calculations also provide useful information about intrinsic and mode coupling anharmonicities. For example, the higher frequency hydrogenic stretching modes were found to tend toward higher intrinsic anharmonicity than anharmonicity due to coupling.

The availability of gas-phase experimental data contributes significantly to the understanding of the suitability of the potential surfaces. A very important conclusion of this study is that spectroscopy can be used to test potential energy surfaces, and in fact, the results support the validity of the modified PM3 potential used here. This suggests further applications of the improved PM3 potential to nucleotide bases and their complexes; while nonadapted PM3 surfaces have already been shown to be viable for molecular dynamics calculations of biological molecules (see, for example, ref 37), it is hoped that the adapted PM3 surface could offer increased accuracy. Additionally, it appears that further improvements in the PM3 method, such as in describing hydrogen bonds,[33,34] may also improve the accuracy.

Most importantly, the power of gas-phase spectroscopy in providing accurate information on increasingly complex biological molecules is evident. It is hoped that additional biological systems can be explored by the combination of high-resolution spectroscopy and harmonic and anharmonic vibrational calculations with high-quality potentials. This should lead to progress in our understanding of the properties of the potential surfaces of biological molecules.

**Acknowledgment.** This material is based on work supported by the National Science Foundation under Grant No. CHE-0244341. Research performed at Hebrew University was conducted under the auspices of the Saerree K. and Louis P. Fiedler Chair in Chemistry. Helpful comments by Dr. Eric C. Brown and Dr. Galina M. Chaban are gratefully acknowledged.

## References and Notes

(1) Simons, J. P. *Phys. Chem. Chem. Phys.* **2004**, *6*, E7.

(2) (a) Snoek, L. C.; Robertson, E. G.; Kroemer, R. T.; Simons, J. P. *Chem. Phys. Lett.* **2000**, *321*, 49−56. (b) Çarçabal, P.; Kroemer, R. T.; Snoek, L. C.; Simons, J. P.; Bakker, J. M.; Compagnon, I.; Meijer, G.; von Helden, G. *Phys. Chem. Chem. Phys.* **2004**, *6*, 4546−4552. (c) Martinez, S. J.; Alfano, J. C.; Levy, D. H. *J. Mol. Spectrosc.* **1992**, *156*, 421−430.

(3) (a) Cable, J. R.; Tubergen, M. J.; Levy, D. H. *J. Am. Chem. Soc.* **1987**, *109*, 6198−6199. (b) Cohen, R.; Brauer, B.; Nir, E.; Grace, L.; de Vries, M. S. *J. Phys. Chem. A* **2000**, *104*, 6351−6355.

(4) See, for example: (a) Nir, E.; Janzen, C.; Imhof, P.; Kleinermanns, K.; de Vries, M. S. *J. Chem. Phys.* **2001**, *115*, 4604−4611. (b) Nir, E.; Grace, L.; Brauer, B.; de Vries, M. S. *J. Am. Chem. Soc.* **1999**, *121*, 4896−4897. (c) Bakker, J. M.; Compagnon, I.; Meijer, G.; von Helden, G.; Kabeláč, M.; Hobza, P.; de Vries, M. S. *Phys. Chem. Chem. Phys.* **2004**, *6*, 2810−2815. (d) Plützer, C.; Hünig, I.; Kleinermanns, K.; Nir, E.; de Vries, M. S. *ChemPhysChem* **2003**, *4*, 838−842. (e) Nir, E.; Janzen, C.; Imhof, P.; Kleinermanns, K.; de Vries, M. S. *Phys. Chem. Chem. Phys.* **2002**, *4*, 732−739. (f) Nir, E.; Kleinermanns, K.; de Vries, M. S. *Nature* **2000**, *408*, 949−951.

(5) (a) Watson, J. D.; Crick, F. H. C. *Nature* **1953**, *171*, 737−738. (b) Franklin, R. E.; Gosling, R. G. *Nature* **1953**, *171*, 740−741.

(6) Watson, J. D.; Crick, F. H. C. *Nature* **1953**, *171*, 964−967.

(7) See, for example: (a) Löwdin, P.-O. *Rev. Mod. Phys.* **1963**, *35*, 724−732. (b) Hanus, M.; Kabeláč, M.; Rejnek, J.; Ryjáček, F.; Hobza, P. *J. Phys. Chem. B* **2004**, *108*, 2087−2097. (c) Kool, E. T.; Morales, J. C.; Guckian, K. M. *Angew. Chem., Int. Ed.* **2000**, *29*, 990−1009. (d) Goodman, M. F. *Proc. Natl. Acad. Sci. U.S.A.* **1997**, *94*, 10493−10495. (e) Noguera, M.; Sodupe, M.; Bertrán, J. *Theor. Chem. Acc.* **2004**, *112*, 318−326. (f) Nedderman, A. N. R.; Stone, M. J.; Williams, D. H.; Lin, P. K. T.; Brown, D. M. *J. Mol. Biol.* **1993**, *230*, 1068−1076. (g) Gorb, L.; Podolyan, Y.; Leszczynski, J.; Siebrand, W.; Fernández-Ramos, A.; Smedarchina, Z. *Biopolymers* **2002**, *61*, 77−83. (h) Podolyan, Y.; Gorb, L.; Leszczynski, J. *Int. J. Mol. Sci.* **2003**, *4*, 410−421. (i) Leszczynski, J. *J. Phys. Chem. A* **1998**, *102*, 2357−2362. (j) Gorb, L.; Podolyan, Y.; Dziekonski, P.; Sokalski, W. A.; Leszczynski, J. *J. Am. Chem. Soc.* **2004**, *126*, 10119−10129. (k) Hossain, M. T.; Sunami, T.; Tsunoda, M.; Hikima, T.; Chatake, T.; Ueno, Y.; Matsuda, A.; Takénada, A. *Nucleic Acids Res.* **2001**, *29*, 3949−3954.

(8) (a) Nir, E.; Müller, M.; Grace, L. I.; de Vries, M. S. *Chem. Phys. Lett.* **2002**, *355*, 59−64. (b) Nir, E.; Hünig, I.; Kleinermanns, K.; de Vries, M. S. *Phys. Chem. Chem. Phys.* **2003**, *5*, 4780−4785.

(9) (a) Nir, E.; Plützer, C.; Kleinermanns, K.; de Vries, M. S. *Eur. Phys. J. D* **2002**, *20*, 317−329. (b) Gerhards, M.; Unterberg, C. *Appl. Phys. A* **2001**, *72*, 273−279.

(10) (a) Šponer, J.; Hobza, P. *Collect. Czech. Chem. Commun.* **2003**, *68*, 2231−2282. (b) Hobza, P.; Kabeláč, M.; Šponer, J.; Mejzlík, P.; Vondrášek, J. *J. Comput. Chem.* **1997**, *18*, 1136−1150. (c) Šponer, J.; Jurečka, P.; Hobza, P. *J. Am. Chem. Soc.* **2004**, *126*, 10142−10151. (d) Shishkin, O. V.; Šponer, J.; Hobza, P.; *J. Mol. Struct.* **1999**, *477*, 15−21. (e) Burda, J. V.; Šponer, J.; Hrabáková, J.; Zeizinger, M.; Leszczynski, J. *J. Phys. Chem. B* **2003**, *107*, 5349−5356. (f) Danilov, V. I.; Anisimov, V. M. *J. Biomol. Struct. Dyn.* **2005**, *22*, 471−482. (g) Kabanov, A. V.; Komarov, V. M.; Yakushevich, L. V.; Teplukhin, A. V. *Int. J. Quantum Chem.* **2004**, *100*, 595−609 and references therein. (h) Jurečka, P.; Nachtigall, P.; Hobza, P. *Phys. Chem. Chem. Phys.* **2001**, *3*, 4578−4582. (i) Hanus, M.; Ryjáček, F.; Kabelář, M.; Kubař, T.; Bogdan, T. V.; Trygubenko, S. A.; Hobza, P. *J. Am. Chem. Soc.* **2003**, *125*, 7678−7688 and references therein. (j) Trygubenko, S. A.; Bogdan, T. V.; Rueda, M.; Orozco, M.; Luque, F. J.; Šponer, J.; Slavíček, P.; Hobza, P. *Phys. Chem. Chem. Phys.* **2002**, *4*, 4192−4203 and references therein.

(11) (a) Florián, J.; Leszczynski, J.; Johnson, B. G. *J. Mol. Struct.* **1995**, *349*, 421−426. (b) Špirko, V.; Šponer, J.; Hobza, P. *J. Chem. Phys.* **1997**, *106*, 1472−1479. (c) Grunenberg, J. *J. Am. Chem. Soc.* **2004**, *126*, 16310−16311.

(12) (a) Woutersen, S.; Cristalli, G. *J. Chem. Phys.* **2004**, *121*, 5381−5386. (b) Krummel, A. T.; Mukherjee, P.; Zanni M. T. *J. Phys. Chem. B* **2003**, *107*, 9165−9169.

(13) (a) Schmidt, M. W.; Baldridge, K. K.; Boatz, J. A.; Elbert, S. T.; Gordon, M. S.; Jensen, J. J.; Koseki, S.; Matsunaga, N.; Nguyen, K. A.; Su, S.; Windus, T. L.; Dupuis, M.; Montgomery, J. A. *J. Comput. Chem.* **1993**, *14*, 1347−1363. (b) http://www.msg.ameslab.gov/GAMESS/GAMESS.html. (c) Chaban, G. M.; Jung, J. O.; Gerber, R. B. *J. Chem. Phys.* **1999**, *111*, 1823−1829. (d) Jung, J. O.; Gerber, R. B. *J. Chem. Phys.* **1996**, *105*, 10332−10348. (e) Stewart, J. J. P. *J. Comput.-Aided Mol. Des.* **1990**, *4*, 1−45.

(14) (a) Werner, H.-J.; Knowels, P. J.; et al. *MOLPRO*, version 2002.6, a package of ab initio programs; Birmingham, U.K., 2002. (b) Rauhut, G. *J. Chem. Phys.* **2004**, *121*, 9313−9322.

(15) (a) Frisch, M. J.; et al. *Gaussian 03*, revision A.1; Gaussian Inc.: Pittsburgh, PA, 2003. (b) Barone, V. *J. Chem. Phys.* **2005**, *122*, 014108.

(16) Chaban, G. M.; Jung, J. O.; Gerber, R. B. *J. Phys. Chem. A* **2000**, *104*, 10035−10044.

(17) Chaban, G. M.; Gerber, R. B. *J. Chem. Phys.* **2001**, *115*, 1340−1348.

(18) Gregurick, S. K.; Chaban, G. M.; Gerber, R. B. *J. Phys. Chem. A* **2002**, *106*, 8696−8707.
(19) Barone, V. *Chem. Phys. Lett.* **2004**, *383*, 528−532.
(20) Barone, V. *J. Phys. Chem. A* **2004**, *108*, 4146−4150.
(21) Barone, V.; Festa, G.; Grandi, A.; Rega, N.; Sanna, N. *Chem. Phys. Lett.* **2004**, *388*, 279−283.
(22) Brauer, B.; Chaban, G. M.; Gerber, R. B. *Phys. Chem. Chem. Phys.* **2004**, *6*, 2543−2556.
(23) Benoit, D. M. *J. Chem. Phys.* **2004**, *120*, 562−573.
(24) (a) Feyereisen, M.; Fitzgerald, G.; Komornicki, A. *Chem. Phys. Lett.* **1993**, *208*, 359−363. (b) Weigend, F.; Häser, M. *Theor. Chem. Acc.* **1997**, *97*, 331−340.
(25) Dunning, T. H., Jr. *J. Chem. Phys.* **1989**, *90*, 1007−1023.
(26) Weigend, F.; Häser, M.; Patzelt, H.; Ahlrichs, R. *Chem. Phys. Lett.* **1998**, *294*, 143−152.
(27) Ahlrichs, R.; Bär, M.; Häser, M.; Horn, H.; Kölmel, C. *Chem. Phys. Lett.* **1989**, *162*, 165−169.
(28) Schaftenaar, G.; Noordik, J. H. *J. Comput.-Aided Mol. Des.* **2000**, *14*, 123−134.
(29) Bode, B. M.; Gordon, M. S. *J. Mol. Graphics Modell.* **1998**, *16*, 133−138.
(30) Meijer, G.; de Vries, M. S.; Hunziker, H. E.; Wendt, H. R. *Appl. Phys. B* **1990**, *51*, 395−403.
(31) (a) Bakker, J. M.; Satink, R. G.; von Helden, G.; Meijer, G. *Phys. Chem. Chem. Phys.* **2002**, *4*, 24−33. (b) Oepts, D.; van der Meer, A. F. G.; van Amersfoort, P. W. *Infrared Phys. Technol.* **1995**, *36*, 297−308.
(32) Abo-Riziq, A.; Grace, L.; Nir, E.; Kabeláč, M.; Hobza, P.; de Vries, M. S. *Proc. Natl. Acad. Sci. U.S.A.* **2005**, *102*, 20−23.
(33) Harb, W.; Bernal-Uruchurtu, M. I.; Ruiz-López, M. F. *Theor. Chem. Acc.* **2004**, *112*, 204−216.
(34) Dannenberg, J. J. *THEOCHEM* **1997**, *401*, 279−286.
(35) Dickerson, R. E.; Bansal, M.; Calladine, C. R.; Diekmann, S.; Hunter, W. N.; Kennard, O.; von Kitzing, E.; Lavery, R.; Nelson, H. C. M.; Olson, W. K.; Saenger, W.; Shakked, Z.; Sklenar, H.; Soumpasis, D. M.; Tung, C.-S.; Wang, A. H.-J.; Zhurkin, V. B. *EMBO J.* **1989**, *8*, 1−4.
(36) Gerber, R. B.; Chaban, G. M.; Brauer, B.; Miller, Y. In *Theory and Applications of Computational Chemistry: the First Forty Years*; Dyskra, C. E., Ed.; in press.
(37) Shemesh, D.; Chaban, G. M.; Gerber, R. B., *J. Phys. Chem. A* **2004**, *108*, 11477−11484.